Physico-Chemical Properties of Ln(III) Complexes

Carlos F. Geraldes

Department of Life Sciences and NMR Laboratory, Center of Neurosciences
University of Coimbra, Portugal

EMMI Intensive Program
"Design, Synthesis and Validation of Imaging probes"
19-30 September, 2011, Torino, Italy

Summary

1. Introduction: history and relative abundances
2. Electronic configuration: ionization energies and oxidation states
3. Spectroscopic properties: magnetic, optical. Applications.
4. Ionic properties: coordination number, radii
5. Reactions with water: hydration, hydrolysis
6. Inorganic complexes - crystal structures by X-ray diffraction
7. Inorganic complexes – solution structures and structural equilibria by NMR

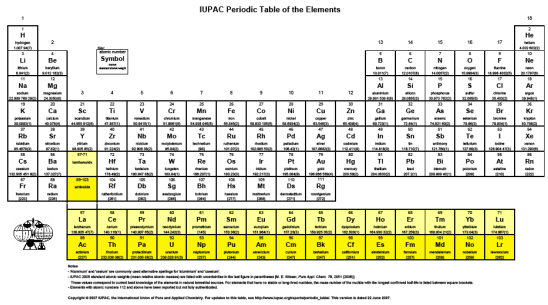

General

Family of elements with similar chemical properties and useful physical properties

Rare earths: Lanthanoids + Y + Sc
Lanthanides: no longer used by IUPAC
Lanthanoids: La-Lu

Physical properties:
- Optical
- Magnetic

Useful for
- Spectroscopy:
- Luminescence
- NMR
- EPR

- Imaging:
- Optical
- MRI

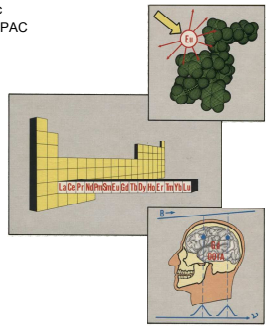

History

1788: "ytterbite" – new black mineral
in old mine (Ytterby, Sweden)
1794: Yttrium - Gadolin

TABLE 1.1

Chronology of Discovery

Year	Name	Discoverers	Origin of Name
1803	Cerium	M. H. Klaproth J. J. Berzelius W. Hisinger	After Ceres, newly discovered asteroid
1839	Lanthanum	C. G. Mosander	From Greek word lanthanein meaning "hidden"
1843	Terbium	C. G. Mosander	After town of Ytterby
	Erbium	C. G. Mosander	After town of Ytterby
1878	Ytterbium	J. C. G. Marignac	After town of Ytterby
1879	Samarium	L. De Boisbaudran	After Russian mine official M. Samarsal
	Holmium	P. T. Cleve	From Latin name of Stockholm, "Holmia"
	Thulium	P. T. Cleve	After ancient name of Scandanavia. "Thule"
1880	Gadolinium	J. C. G. Marignac	After J. Gadolin, discoverer of Yttrium
1885	Praseodymium	C. A. von Welsbach	From Greek words prasios and didymos which mean "green twin"
	Neodymium	C. A. von Welsbach	From Greek words neos and didymos meaning "new twin"
1886	Dysprosium	L. de Boisbaudran	From Greek word dysprositos which means "hard to obtain"
1889	Europium	W. Crookes	After Europe
1907	Lutetium	G. Urban C. A. Welsbach	After Latin name of Paris, "Lutetia"
1947	Promethium	J. A. Marinsky L. E. Glendenin C. D. Coryell	From Prometheus who gave fire to man

Relative abundances

Rare earths are not rare: > 100 minerals: monazite (Ln-Th), cerite (Ce), gadolinite (Gd), …
Abundance: 1) decreases with Z increase
2) Odd-even effect: La (Z = 57) < Ce (Z= 58) > Pr (Z = 59)

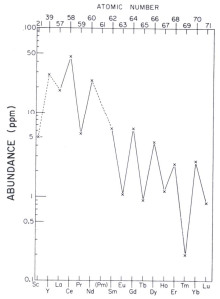

Fig 1.1 The pattern of elemental abundances for the rare earth elements.

Electronic configuration

TABLE 1.2

Ground State Electronic Configuration

Element	Ln^0	Ln^{2+}	Ln^{3+}	Ln^{4+}
La	$5d^16s^2(^2D_{3/2})$		$4f^0(^1S_0)$	
Ce	$4f^15d^16s^2(^3G_4)$		$4f^1(^2F_{5/2})$	$4f^0(^1S_0)$
Pr	$4f^36s^2(^4I_{9/2})$		$4f^2(^3H_4)$	$4f^1(^2F_{5/2})$
Nd	$4f^46s^2(^5I_4)$		$4f^3(^4I_{9/2})$	
Pm	$4f^56s^2(^6H_{5/2})$		$4f^4(^5I_4)$	
Sm	$4f^66s^2(^7F_0)$	$4f^6(^7F_0)$	$4f^5(^6H_{5/2})$	
Eu	$4f^76s^2(^8S_{7/2})$	$4f^7(^8S_{7/2})$	$4f^6(^7F_0)$	
Gd	$4f^75d^16s^2(^9D_2)$		$4f^7(^8S_{7/2})$	$4f^7(^8S_{7/2})$
Tb	$4f^96s^2(^6H_{15/2})$		$4f^8(^7F_6)$	
Dy	$4f^{10}6s^2(^5I_8)$		$4f^9(^6H_{15/2})$	
Ho	$4f^{11}6s^2(^4I_{15/2})$		$4f^{10}(^5I_8)$	
Er	$4f^{12}6s^2(^3H_6)$		$4f^{11}(^4I_{15/2})$	
Tm	$4f^{13}6s^2(^2F_{7/2})$		$4f^{12}(^3H_6)$	
Yb	$4f^{14}6s^2(^1S_0)$	$4f^{14}(^1S_0)$	$4f^{13}(^2F_{7/2})$	
Lu	$4f^{14}5d^16s^2(^3D_{3/2})$		$4f^{14}(^1S_0)$	

- Lanthanide compounds have very **similar chemical properties** – in part due to common **Ln^{3+} sta**
- Relative energies of 4f, 5d, 6s and 6p orbitals for Z = 57-71 elements
- The **4f** orbitals have **lower energy** than **6s** and **5d**

Ionization energies

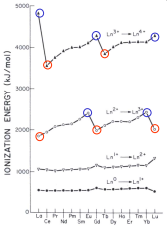

Fig 1.2 Ionization energies for successive ionization steps of the lanthanide gaseous species.

Ln^0 → Ln^+ and Ln^+ → **Ln^{2+}** quite constant with Z: ionizing 6s electrons

Ln^{2+} → Ln^{3+} vary with Z:
- removal of 5d electron (La, Ce, Gd, Lu) - low energy
- removal of 5f electron (Pr, Nd, Pm, Sm, Eu, Tb, Dy, Ho, Er, Tm, Yb) - high energy
- gives Ln^{3+} with configuration $4f^n$ (n = 0 - 14)
- maximum stability for **Eu^{2+}** and **Yb^{2+}** (n = 7, 14): stable S states – Hund's rule

Ln^{3+} → Ln^{4+} vary with Z:
- high for La, Gd, Lu (n = 0, 7, 14): Ln^{3+} stable S states – Hund's rule
- maximum stability for **Ce^{4+}** and **Tb^{4+}** for the same reason

Redox potentials

Stability of oxidation state in water depends on balance of **ionization energy** and **hydration energy**

$$Ln_{(g)} \rightarrow Ln^{3+}_{(g)} + 3e \qquad \Delta H = I_1 + I_2 + I_3$$

$$Ln^{3+}_{(g)} + n\,H_2O \rightarrow Ln^{3+}_{(aq)} \qquad \Delta H = \Delta H_{hyd}$$

TABLE 1.3

Reduction Potentials (volts)

Element	Acidic Solution (III)/(0)	(III)/(II)	(IV)/(III)	Basic Solution (III)/(0)	(IV)/(III)
La	-2.37			-2.80	
Ce	-2.34		+1.72	-2.78	-0.7
Pr	-2.35		+3.2	-2.79	+0.8
Nd	-2.32			-2.78	
Pm	-2.29			-2.76	
Sm	-2.30	-1.55		-2.80	
Eu	-1.99	-0.35		-2.51	
Gd	-2.29			-2.82	
Tb	-2.30		+3.1	-2.82	+2.3
Dy	-2.29			-2.80	
Ho	-2.33			-2.85	
Er	-2.32			-2.84	
Tm	-2.31			-2.83	
Yb	-2.22	-1.05		-1.74	
Lu	-2.30			-2.83	

- Ln^{3+} most stable
- Eu^{2+} (Yb^{2+}) and Ce^{4+} (Tb^{4+}) have some stability (from ionization potentials – see E^0)

Magnetic properties

Ln^{3+} are **paramagnetic** except La^{3+} (f^0) and Lu^{3+} (f^{14})

Magnetic moments: orbital and spin contributions
Maxima at Pr-Nd and Dy-Ho

Magnetic moment proportional to magnetic susceptibility:

$$\chi_m = Ng^2\beta^2 J(J+1)/3kT$$

J = L+S (no quenching of L because f orbitals are inner and shielded from ligand field)

Sm^{3+} and Eu^{3+} have contribution from low lying excited states with different J values within the ground state term ($^{2S+1}L_J$)

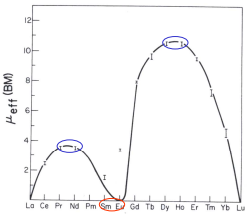

Fig 1.3 Experimental values of the magnetic moments, in Bohr magnetons, of the trivalent lanthanide ions; the solid line is calculated from eq. 1.

Anisotropic magnetic susceptibility leads to NMR dipolar shifts

Paramagnetic NMR shifts

Pseudo-contact or dipolar shift: results from local magnetic field at nucleus caused by anisotropic susceptibility of Ln^{3+} complex averaged by its rotation in solution

$$\Delta_p = \frac{C_J \mu B^2}{60k^2T^2}\left[\frac{\langle r^{-3}\rangle A_0^2(3\cos^2\theta - 1)}{r^3} + \frac{\langle r^{-3}\rangle A_2^2 \sin^2\theta\cos 2\varphi}{r^3}\right]$$

$$\Delta_p = D_1\frac{3\cos^2\theta - 1}{r^3} + D_2\frac{\sin^2\theta\cos 2\varphi}{r^3} = D_1G_1 + D_2G_2$$

r, θ, and φ = spherical coordinates of nucleus in the coordinate system of the Ln3+ at the origin
G_1 and G_2 = axial and rhombic geometric terms and
D_1 and D_2 are proportional to the axial and transverse anisotropies of χ_m
In the case of axial symmetry only the first term remains (D_2 =0), giving **structural information**

Contact shift: through-bond transmission of unpaired spin from Ln 4f orbitals to nucleus

$$\Delta_c = \langle S_z\rangle F = \langle S_z\rangle \frac{A}{\hbar\gamma_n B_0}10^6$$

$\langle S_z\rangle$ = expectation value of S_z, $A/\hbar$ = hyperfine coupling constant; effect disappears after a few bonds

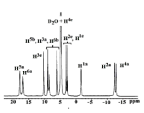

Nddo2a2p

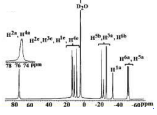

Ybdo2a2p

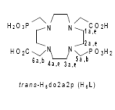

trans-$H_5do2a2p$ (H_5L)

Geraldes et al, *Chem Eur J.*, 16, 8446-65 (2010)

Determine hydration numbers of Ln^{3+} complexes using ^{17}O paramagnetic NMR shifts

^{17}O NMR shift of water in a Ln^{3+}-complex with coordination number q:

$$\Delta = q\cdot\delta_{dia} + q\cdot\langle S_z\rangle\cdot F + q\cdot C^D\cdot G$$

Paramagnetic shift dominated by contact term

$$F = \frac{\beta}{3kTy_O}\cdot\frac{A}{\hbar}\cdot 10^6 = \frac{6.172\cdot 10^{-3}}{T}\cdot\frac{A}{\hbar}$$

F and *(A/h)* independent of the complex and of the type of ^{17}O

$$\frac{A}{\hbar} \approx -(3.9\pm 0.3)\pm 10^6\,\mathrm{rad\,s^{-1}} \quad \rightarrow \quad F \approx \frac{-2.407\cdot 10^4}{T}$$

$$\Delta_{para} = \Delta - q\cdot\delta_{dia} = q\cdot\langle S_z\rangle\cdot F + q\cdot C^D\cdot G$$

$$\frac{\Delta_{para}}{C^D} = \frac{\Delta - q\cdot\delta_{dia}}{C^D} = \frac{q\cdot\langle S_z\rangle}{C^D}F + q\cdot G$$

Practical method: ^{17}O DyIS
^{17}O DyIS is 85% contact
(^{17}O shift vs p_r (Dy-ligand)

Figure 1. Plots of Δ_{para}/C^D vs $q\cdot\langle S_z\rangle/C^D$. $F + q\cdot G$ for the series of Ln(III) trifluoromethanesulfonates (triflates). The samples were measured at 54.1 MHz and 25 °C. The values for Gd(III) and Sm(III) are not included because of the small C^D of these lanthanides.

Figure 2. DyIII ^{17}O NMR induced shift vs the molar ratio DyIII/ligand (a_r) for 0.05 *m* solution of complex in D_2O at 76°C.

In a series of Ln-complexes the plot has breaks if q changes
Ln^{3+} (aq): Ce- Nd (q =9); Tb-Yb (q =8)

Geraldes, Peters, *Dalton Trans.* 463–46 (1992)
Peters, *Contrast Media Mol. Imaging* 2, 67–71 (2007)

Optical properties

Absorption or emission (luminescence) spectra involving electronic states of Eu^{3+} and Tb^{3+}

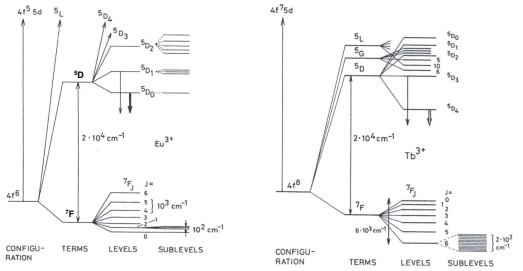

Fig. 7.2 Partial energy diagrams for Eu(III), $4f^6$ (top) and Tb(III), $4f^8$ (bottom) ions showing the relative magnitude of the interelectronic repulsion, spin-orbit coupling, and ligand-field effects. Downward arrows indicate the most luminescent excited levels.

Absorption spectra – UV/vis

f → f electronic transitions:
- Minimal perturbation by ligand field:
- **Narrow**
- λ almost independent of complexation (visible)
- **Weak** intensity (forbidden by parity or **Laporte rule**: unsymmetrical movement of charge)
- Can get intensity from low symmetry or vibronic coupling
- Some transitions are **hypersensitive**

eg: Eu^{3+} J = 0, 1, 2, 3, 4, 5, 6 (^7F_J)

f → d electronic transitions:
- Intense (allowed)
- near-UV or visible

TABLE 1.4

Principal f → f (Laporte forbidden) Absorption Bands of Ln^{3+} in H_2O/D_2O Solutions ($\epsilon \geq 0.2$ l mol^{-1} cm^{-1})

Trivalent Ion	Unpaired Electrons	Absorption Bands (nm)	Color
La	0	none	colorless
Ce	1	none	colorless
Pr	2	444.5, 469.0, 482.2, 588.5	green
Nd	3	345.0, 521.8, 574.5, 739.5, 742.0, 797.5, 803.0, 868.0	rose
Pm	4	548.5, 568.0, 702.5, 735.5	pink
Sm	5	362.5, 374.5, 402.0	yellow
Eu	6	375.5, 394.1	very pale pink
Gd	7	272.9, 273.3, 275.4, 275.6	colorless
Tb	6	284.4, 350.3, 367.7, 487.2	very pale pink
Dy	5	300.4, 345.0, 910.0	yellow
Ho	4	287.0, 361.1, 416.1, 450.8, 537.0, 641.0	yellow
Er	3	364.2, 379.2, 487.0, 522.8, 652.5	rose
Tm	2	360.0, 682.5, 780.0	green
Yb	1	975.0	colorless
Lu	0	none	colorless

Absorption vs Luminescence

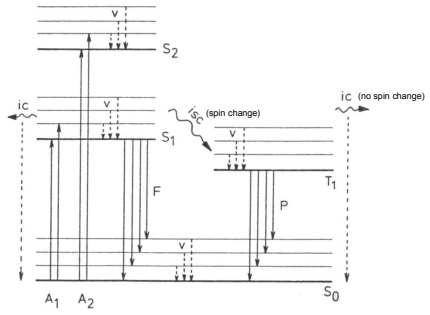

Fig. 7.1 Two-electron system undergoing various transitions : S_i = singlet state, T_i = triplet state, A = absorption, v = vibrational relaxation, ic = internal conversion, isc = intersystem crossing, F = fluorescence, P = phosphorescence.

Luminescence spectra

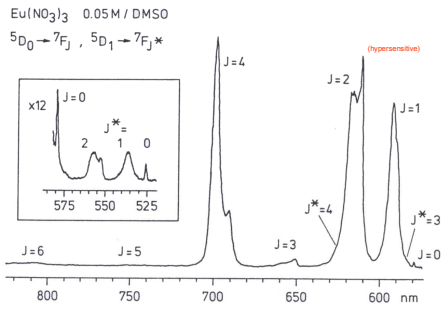

Fig 7.3 Luminescence spectrum of a solution of $Eu(NO_3)_3$ 0.05 M in dimethylsulfoxide. Excitation : $^5L_6$ level (394 nm). Vertical scale : arbitrary units (note the 12-time magnification in the inset). Analyzing bandpass : 0.3 nm.

Luminescence spectra

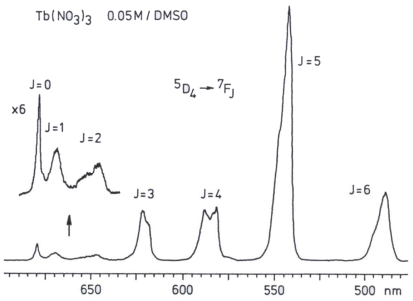

Fig. 7.4 Luminescence spectrum of a solution of $Tb(NO_3)_3$ 0.05 M in dimethylsulfoxide. Excitation : 368 nm. Vertical scale : arbitrary units. Analyzing bandpass : 0.3 nm.

Luminescence spectra

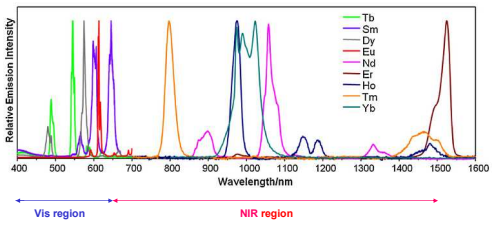

Normalized emission spectra of luminescent lanthanide complexes in solution, illustrating the sharp emission bands and minimal overlap of lanthanide luminescence

Ln luminescence spectra

Advantages relative to organic dyes:

- Very long luminescence lifetimes: 10 μsec to several hundred msec
- Very sharp emission bands
- No bleaching

Disadvantages:

- Low intensity absorption

To obtain more intense luminescence, can used direct excitation using LASERS or sensitized luminescence

Sensitized luminescent Ln complexes

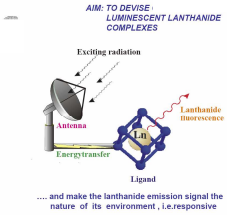

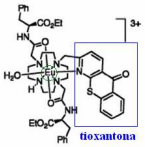

- Exciting UV radiation is absorbed by ligand aromatic chromophore (antenna)
- Energy transfer from ligand to Ln^{3+} ion via intramolecular ISC (depends on d^{-6})
- Energy emission due to visible f-f transitions at the Ln^{3+} ion

High luminescence intensity, large Stokes shifts

Excitation and sensitized emission spectra

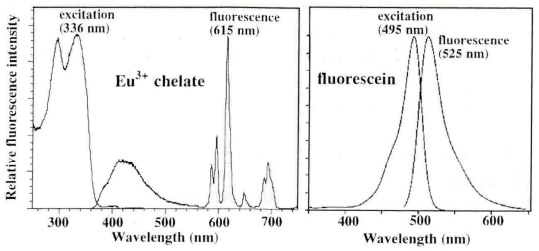

FIG. 1. Excitation and emission spectra of the Eu^{3+} chelate with *N,N,N',N'*-[(4'-phenyl-2,2':6',2"-terpyridine-6,6"-diyl)bis(methylenenitrilo)]tetrakis(acetate) (left) and fluorescein (right).

Energy transfer – sensitized luminescence

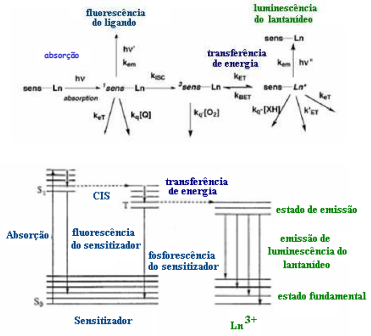

Luminescence lifetimes for Eu^{3+} and Tb^{3+}

Weak vibronic coupling of Ln^{3+} excited states with OH oscillators of bonded H_2O molecules leads to radiationless deexcitation of Ln^{3+} → lifetimes decrease

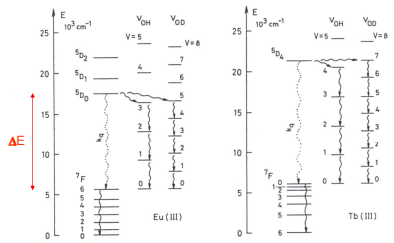

Fig. 7.10. Radiationless deexcitation of Eu(III) and Tb(III) ions by OH and OD oscillators.

Quenching effect strongly **decreases** with **increase** of d(Ln-OH) oscillator and of Ln ΔE energy gap (requires promotion of OH oscillator to low populated higher vibrational harmonic v – Franck-Condon energy match). This effect is much more pronounced for O-D oscillators (lower ν_{OD}): ($k_{H2O} \sim 200\ k_{D2O}$)

Determine hydration numbers of Eu^{3+}/Tb^{3+} complexes

Quenching of excited state is proportional to hydration number

In H_2O: $k_{obs} = k^0_F + \Sigma\, k_i^{nr} + k_{H2O}\, x_{H2O}$ Large isotope effect ($k_{D2O} << k_{H2O}$), use H_2O/D_2O

In D_2O : $k_{obs} = k^0_F + \Sigma\, k_i^{nr}$

$\Delta k_{obs} = k_{obs}(H_2O) - k_{obs}(D_2O) = C' \,.\, N$ → **n = C . Δk_{obs} (Horrocks method)**

(also contributions from CH/CD, NH/ND - Parker)

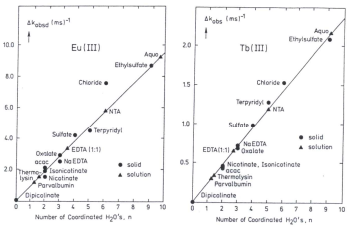

Fig. 7.11. Plots of Δk_{obsd} vs. the number n of coordinated water molecules. Adapted from ref. 33.

Ionic properties

Coordination number and geometry

- **Highly variable: CN = 3 – 12 (8-9 most common)**
- **Ionic bonds** in Ln(III) complexes

➔ Coordination geometry reflects balance of **electrostatic** and **steric** interactions

Ionic properties

Ionic radii

-**"Effective" ionic radii (Shannon) depend on CN (6, 8, 9)**
- **Small decrease with Z**
(lanthanide contraction)

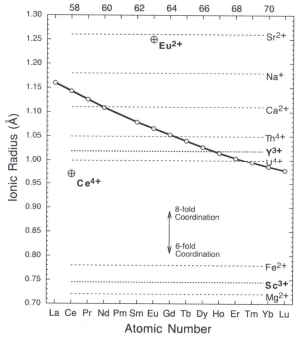

Reactions with water

Hydrolysis

- **Hydrolysis in water above pH 6:**

$$Eu^{3+}_{(aq)} + H_2O_{(l)} \Leftrightarrow Eu(OH)^{3+}_{(aq)} + H^+$$

Hydrolysis constant: $\beta_1^* = [Eu(OH)^{2+}][H^+]/[Eu^{3+}]$

log β_1^* = - 8.5 (La) to – 7.6 (Lu) at I = 0 ➔ **hydrolysis easier for smaller Lu^{3+} ion**

At pH 7 ➔ **$[Ln(OH)^{2+}] \sim [Ln^{3+}]$**

Reactions with water

Hydration

– **ΔH_{hyd} of Ln^{3+} increases with Z**
(smaller radius, higher charge density, stronger ion-dipole interaction)
- **Primary coordination sphere: most common CN = 8-9**

- **$[Ln(H_2O)_9]^{3+}$** in bromates and ethylsulfates,
eg. $[Nd(H_2O)_9]^{3+}$: **tricapped trigonal prism**
Capped square antiprism almost as stable

-**$[Ln(H_2O)_8]^{3+}$: square antiprism**

- **In solution:** CN changes along Ln series: CN = 9 (La-Nd); 8/9 (Sm-Tb); 8 (Dy-Lu)
- Large second sphere of hydration

Ln(III)(aq) geometries : theoretical calculations

Ab initio QM calculations
Structures with small ΔE

$[Gd(H_2O)_8]^{3}$

Stability

SAP (b) > Dodeca (c) > SP (a)

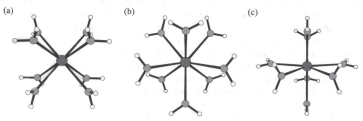

Figure 7.1 Different geometries of $Gd(H_2O)_9^{3+}$: (a) cube; (b) square-antiprism; (c) dodecadeltahedron.

$[Gd(H_2O)_9]^{3}$

Stability

TTP D_{3h} > TTP D_{3d} > TTP C_{3v}

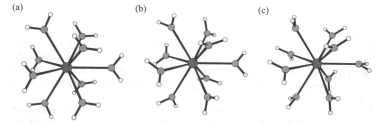

Figure 7.2 Tri-capped trigonal prismatic geometries of $Gd(H_2O)_9^{3+}$ ions with (a) D_{3h}, (b) D_3 and (c) C_{3v} symmetries.

Ln(III)(aq) geometries: X-ray crystal structures

Ln triflates: $[Ln(H_2O)_9(CF_3SO_3)_3]$

$[Ln(H_2O)_9]^{3+}$ (Ln = La-Tm is TTP)
Along series all Ln-O bond lenghts decrease
but **Δ = d (Ln-O)(cap) – d(Ln-O)(prism)** increase;
transition to CN = 6

Ln perchlorates: $[Ln(H_2O)_8(ClO_4)_3]$
Octahedral $[Ln(H_2O)_8]^{3+}$

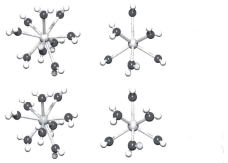

FIG. 1. Views oblique to (left) and along (right) the effective C_3 axis of the $[Ln(OH_2)_9]^{3+}$ cation in hydrated lanthanide triflates, Ln = La (top) and Lu (bottom) [18].

$[Ln(H_2O)_8]^{3+}$ (Square antiprism: SAP)

Triflates: $[Yb(H_2O)_8(CF_3SO_3)_3]$
Bromides: $[Ln(H_2O)_8(CF_3SO_3)_3]$ (Ln = Ho, Lu)

X-ray crystal structures: complexes with neutral ligands

Neutral ligands L = pno, dmso, dmf
decrease CN to 8 (SAP) or 7 due to steric repulsions

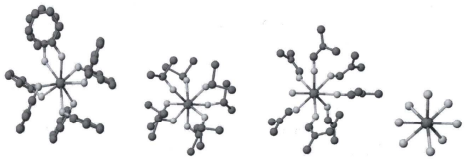

FIG. 2. Eight-coordinate, square antiprismatic Ln(III) complex ions observed in the solid state: (from left to right) $[La(pyridine\text{-}N\text{-}oxide)_8]^{3+}$ [41], $[Gd(dmso)_8]^{3+}$ [35], $[Ho(dmf)_7(OH_2)]^{3+}$ [38] and $[Lu(OH_2)_8]^{3+}$ [31]. (The last figure is not to the same scale. Some distortions from a regular geometry are apparent in all.)

Complexes with simple anions

Small anionic ligands
$L = SO_4^{2-}$ CN = 12, 9, 8,…
$L = ClO_4^-$ CN 9 → 8 (SAP) along series
$L = NO_3^-$: CN 10 → 9 $Ln(NO_3)_3(H_2O)_x$ (x = 4,3)

Large anionic organic ligands
$L = TsO$ ($pCH_3C_6H_4SO_3^-$)
CN 9 (La-Nd) → 8 (SAP) (Sm-Lu)

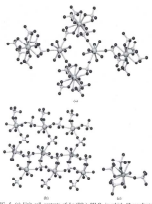

FIG. 3. Aqua-nitrato complex ion species present in crystalline lanthanide nitrate hydrates ([49] and references therein).Top: stereoisomeric forms of 10-coordinate Ln(III) present in $[Tb(NO_3)_3(OH_2)_4]\cdot 2H_2O$ and $[Yb(NO_3)_3(OH_2)_4]\cdot H_2O$. Bottom: stereoisomeric forms of 9-coordinate $[Ln(NO_3)_3(OH_2)_3]$.

FIG. 4. Essentially square antiprismatic forms of 8-coordinate Ln(III) in (from left to right) $[Pr(OH_2)_4(pic)_2]^+$ (pic = 2,4,6-trinitrophenoxide) [53], $[Pr(OH_2)_4Br_2]^+$ [31] and $[Lu(OH_2)_4(tos)_2]^+$ [21] (tos = 4-methylbenzenesulfonate). Non-oxygen atoms are shown as dark spheres, with only the first atom bound to donor-O in pic⁻ and tos⁻ ligands shown.

Complexes with simple anions

L = acetate AcO^-
L = diethyl phosphate ($pCH_3C_6H_4SO_3^-$)

CN = 9
Dimeric, polymeric; bridging groups

FIG. 6. (a) One of the centrosymmetric dimer units, here containing 9-coordinate La(III), making part of the coordination polymer present in crystalline $La(OAc)_3\cdot 1.5H_2O$. (b) The centrosymmetric dimer unit, containing 9-coordinate Lu(III), constituting the binuclear molecule present in $Lu(OAc)_3\cdot 4H_2O$ [63].

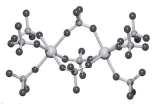

FIG. 7. Part of the polymeric chain of octahedral Nd(III) centres triply bridged by diethylphosphate units in $[Nd((CH_3CH_2O)_2PO_2)_3]$ [70]. (Ethyl groups on the uncoordinated phosphate oxygen atoms omitted for clarity.)

Complexes with hydroxide: hydrolysis

L = OH^-: large clusters containing oxo/hydroxo ligands
CN = 9

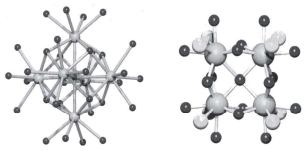

FIG. 8. Clusters formed by oxo/hydroxo ligand bridging of Ln(III): (a) an $Nd_6O(OH)_8$ unit (metal and donor atoms only) produced by hydrolysis of $Nd(ClO_4)_3$ [75]. (b) an $Nd_4(OH)$ unit (the bridging oxygen and unidentate sulfur donors are derived from two thiacalixarene ligands forming a sandwich about the cluster, the terminal atoms from coordinated solvent) [81].

Complexes with neutral multidentate ligands amines, heteroaromatics, sugars

Aliphatic amines (organic solvents) : **L = TMDA** **$[GdCl_3(thf)_2(TMDA)]$ CN = 7, Gd-N > Gd-O**

Aza-aromatic ligands: L = bpy, phen, tpy
Small anion competition: $[Ln(tpy)(O_2NO)_2(OH_2)_n]NO_3\cdot xH_2O$ (n = 3, x = 0, Ln = La-Gd; n = x = 2, Ln = Tb-Lu) (CN = 10,9)

But not for perchlorate: $[Ln(tpy)_3](ClO_4)_3$ (CN = 9: TTP)

Sugar ligands: tridentate 1,3,5-triaxial
1,2,3-ax,eq,ax 6-membered rings

Cyclitols: L = cyclohexanetriols

ML_2 and ML

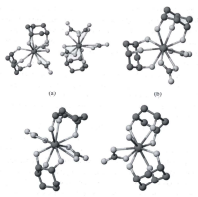

FIG. 9. Metal entities present in crystalline complexes of cyclohexanetriols [95]: (a) The complex ion pair obtained by crystallization of the $La(NO_3)_3$ complex of 1,3,5-cyclohexanetriol from acetonitrile; (b) the cation formed by crystallization from 1,2-dimethoxyethane; (c) the cation present in the complex of $Pr(NO_3)_3$ with 1,2,3-cyclohexanetriol; (d) the cation present in the $Yb(NO_3)_3$ complex of 1,3,5-cyclohexanetriol.

Complexes with funtionalized amines and macrocyclic N or (N,O) mixed ligands

CN = 8, q = 2

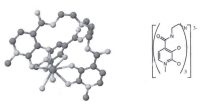

FIG. 13. 8-coordinate Gd(III) in $[Gd(L)(OH_2)_2]_3$ where L is the podand *tris*(hydroxypyridonate) trianionic ligand shown to the right [114].

CN = 12, q = 0 **CN = 10, q = 2**

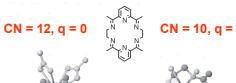

FIG. 14. Ln(III) complexes of the sexidentate macrocycle, L' (inset), $[La(L')(NO_3)_3]$ (left) and $[Nd(L')(OH_2)_2(NO_3)]^+$ (right), in which the macrocycle conformation differs considerably [116b].

CN = 8, q = 0 **CN = 12, q = 0**

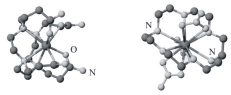

FIG. 16. Ln(III) complexes of mixed-donor (N,O) macrocyclic ligands: left, the 8-coordinate cation present in $[La(DOTPAM)](CF_3SO_3)_3$ [153], and, right, the complex $[La(NO_3)_3(diaza\text{-}18\text{-}crown\text{-}6)]$ containing 12-coordinate La [147a].

Ce(IV): CN = 8, CN = 10

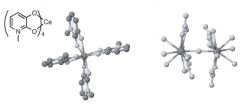

FIG. 15. Left, 8-coordinate Ce(IV) in an hydroxypyridonate complex (formula inset) [134] and, right, 10-coordinate Ce in a dimeric hydrolysis product of $[Ce(NO_3)_6]^{2-}$, $[Ce_2O(NO_3)_8(OH_2)_6]$ [142].

Complexes with simple linear aminocarboxylates

Dipicolinate: L = dipic)
ONO tridentate binding: **$[Ln(dipic)_3]^{3-}$**
CN = 9, TTP
N in capping positions
O in prismatic positions

Similar structures:
L = ida,oxydiacetate, chelidamate

TTP

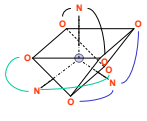

$[Eu(dipic)_3]^{3-}$

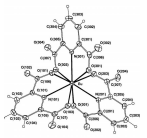

α-aminoacids:
oligomeric, polymeric OH- bridged complexes

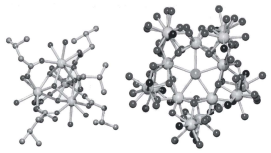

FIG. 12. (a) The $Sm_4(OH)_4^{8+}$ cluster in $[Sm_4(\mu_3\text{-}OH)_4(gly)_8(OH_2)_{11}(ClO_4)_1(ClO_4)_7 \cdot NaClO_4$ [10] (gly = glycinate). (b) The metal/donor atom array, including the "templating" chloride ion and showing the fusion of $Eu_4(OH)_4^{8+}$ units in $[Eu_{17}Cl(\mu_3\text{-}tyr)_{10}(\mu_3\text{-}OH)_{20}(\mu\text{-}OH_2)_{12}(OH_2)_8](ClO_4)_{27} \cdot 56H_2O$ [108] (tyr = L-tyrosinate).

Complexes with linear polyaminopolycarboxylates

L = EDTA: $[Ln(EDTA)(OH_2)_n]^-$ CN = 10 (La), 9, 8; depends on counterion M^+: Ln = Ho; M = K (CN = 9); M = Cs (CN = 8)
dimeric, Cs^+ bridge

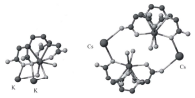

FIG. 10. Partial views of the coordination polymers present in the complexes $K[Ho(EDTA)(OH_2)_2] \cdot 2H_2O$ and $Cs[Ho(EDTA)(OH_2)_2] \cdot 3H_2O$ [103], showing bridging to occur for K^+ (a) via water and inner carboxylate oxygen atoms and for Cs^+ (b) by inner and outer carboxylate oxygen atoms. The full coordination spheres of the alkali metal ions are not shown.

L = DTPA: monomer $[Ln(DTPA)(OH_2)]^{2-}$ CN = 9 (La - Lu) **TTP**
Two enantiomers in asymmetric unit
Backbone stereoisomers also in solution (NMR)

Dimer: carboxylate bridge

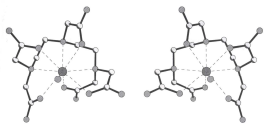

Figure 7.3 Enantiomers of $Gd(DTPA)(H_2O)^{2-}$ (top view); hydrogen atoms are omitted for clarity.

δδ / λλ backbone conformations

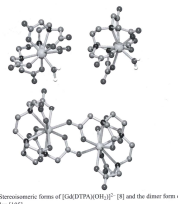

FIG. 11. Stereoisomeric forms of $[Gd(DTPA)(OH_2)]^{2-}$ [8] and the dimer form of the complex [105].

Solution structures and isomers by NMR

Ln-DTPA isomers

^{1}H NMR spectra of Pr-DTPA
vs temperature

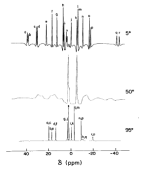

^{1}H 2D- EXSY

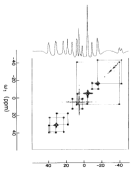

^{13}C NMR spectra of Nd-DTPA vs temp

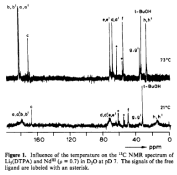

Figure 1. Influence of the temperature on the ^{13}C NMR spectrum of $La_2(DTPA)$ and Na^{III} (p = 0.7) in D_2O at pD 7. The signals of the free ligand are labeled with an asterisk.

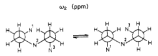

Figure 3. Conformational interconversion in the diethylenetriamine backbone of $Ln(DTPA)^{2-}$ complexes.

- ^{1}H NMR spectra: 18 signals at low temperature become 9 at high temperature
- Complex has TTP structure
- Central N bound to Ln is chiral: an entiomeric pair of diasteroisomers (backbone structures δδ ⇔λλ in exchange)
- ^{13}C NMR spectra also simplify at high temperature

Lauffer, Inorg Chem, 27, 4730-8 (1988)

Peters, *Inorg Chem*, 27, 4686-91 (1988)

Ln DTPA bis-amides in solution by NMR

^{13}C NMR spectra of Nd-DTPA-PA_2 vs temp

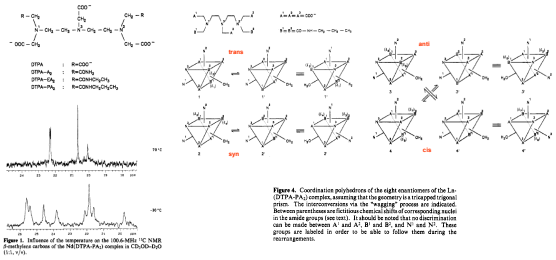

Figure 5. Influence of the temperature on the 100.6-MHz ^{13}C NMR *N*-methylene carbons of the Nd(DTPA-PA_2) complex in CH_3OD–D_2O (1:1, v/v).

Figure 4. Coordination polyhedrons of the eight enantiomers of the Ln-(DTPA-PA_2) complex, assuming that the geometry is a tricapped trigonal prism. The interconversions via the "wagging" process are indicated. Between parentheses are fictitious chemical shifts of corresponding nuclei in the amide groups (see text). It should be noted that no discrimination can be made between A' and A'', B' and B'', and N' and N''. These groups are labeled in order to be able to follow them during the rearrangements.

- **^{13}C NMR spectra show presence of various isomers, number decreases to about half at high temperature**
- **TTP structure: three chiral N atoms ➔ 4 diasteroisomeric pairs of enantiomers: trans -1,1'; syn – 2,2'; anti – 3,3'; cis – 4,4'**
- **Central N3 in a prismatic position, terminal N1 and N3 at capping positions**
- **Dynamics shown in spectra - two processes:**
  1) **racemization of terminal Ns with decoordination of N and neighboring acetates (slow)**
  2) **Interconversion δδ ⇔λλ of backbone en groups (faster)**

Geraldes, Peters, *Inorg Chem*, 32, 2426-32 (1993)

Complexes with macrocyclic polyaminopolycarboxylates

L = DOTA, DOTMA: $[Ln(DOTA)(OH_2)]^-$ CN = 9 **CSAP**
DO3A, DO3MA: $[Ln(DO3MA)(OH_2)_2]^-$ CN = 9 **CSAP**
2 diastereoisomeric pairs; assymetry in ring and arms
CSAP and TCSAP

In solution the ratio changes along the Ln series
For Yb, Lu, CN = 8 also appears with low population

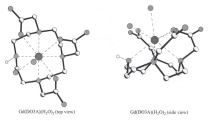

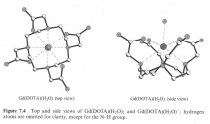

Figure 7.4 Top and side views of $Gd(DOTA)(H_2O)_2$ and $Gd(DOTA)(H_2O)^-$; hydrogen atoms are omitted for clarity, except for the N–H group.

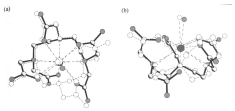

Figure 7.5 Superimposition of $Gd(DTPA)(H_2O)^{2-}$ and $Gd(DOTA)(H_2O)^-$, showing (a) top and (b) side views.

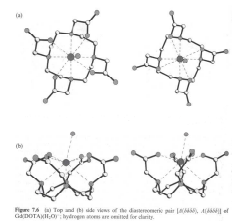

Figure 7.6 (a) Top and (b) side views of the diastereomeric pair [*λλδδδ*, *δδδδδ*] of $Gd(DOTA)(H_2O)^-$; hydrogen atoms are omitted for clarity.

Ln-DOTA isomers in solution by NMR

^{1}H 2D- EXSY spectrum of YbDOTA

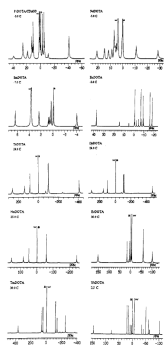

Figure 2. * NMR spectra of paramagnetic LnDOTA$^-$ complexes.

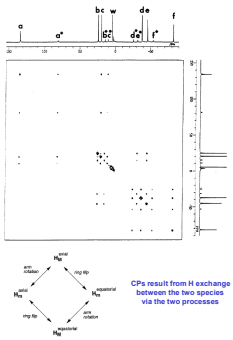

CPs result from H exchange between the two species via the two processes

Two species in equilibrium

Aime, Botta, *Inorg Chem*, 31, 4291-9 (1992)

Ln-DOTA isomers in solution by NMR

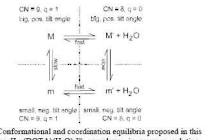

Figure 2. Conformational and coordination equilibria proposed in this work for the $[Ln(DOTA)(H_2O)_q]^{n-}$ complexes in aqueous solution. Enantiomeric pairs are not represented.

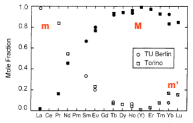

Figure 3. Molar fractions of the isomers M (open symbols), m' (barred symbols), and M (filled symbols) of $[Ln(DOTA)(H_2O)_q]^{n-}$ as a function of the complexed metal ion from ^1H-NMR spectroscopy (0.15 M Ln(DOTA)$^{n-}$, pH 7.0, T = 298 K, ionic strength = 0.1 M): (squares) Aime et al., this work; Tosato, (circles) Hoeft and Roth, T. U. Berlin.[9]

In solution the isomer ratio changes along the Ln series
For Yb, Lu, CN = 8 also appears with low population
(from pressure dependence of 1H NMR isomer populations)

TSAP (m)

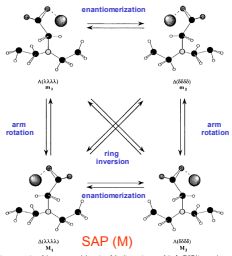

SAP (M)

1. Schematic representation of the structure and dynamics of the diastereoisomers of the $Ln(DOTA)^{n-}$ complexes.

Aime, Botta, Geraldes, Merbach, *Inorg Chem*, 36, 2059-68 (1997)

Factors affecting SAP/TSAP ratio

- **Inner sphere water exchange rate ($k_{ex(H2O)}$) of TSAP isomer is 1- 2 orders of magnitude faster that for SAP**
  (Aime, Parker et al, *Angew Chem Int Ed*, 37, 2673-2675 (1998); Aime, Parker et al, *JACS*, 121, 5762-71 (1999); Aime, Merbach, et al, JACS, 122, 1506-12 (2000)
- **For T_1 GdL CAs, requiring fast exchange rate to have large r_1 relaxivity, TSAP isomer should predominate**
- **For PARACEST Ln-DOTA tetraamides, requiring very slow exchange rate, SAP isomer should predominate**

1) How to determine SAP/TSAP in solution for a given complex?

Chemical shifts of axial ring protons (ax^S) in DOTA-like Ln complexes are very different from others; can be used to identify and quantify the coordination isomers

Ex: for EuDOTA, ax^S (SAP) = 38 ppm; ax^S (TSAP) = 15 ppm

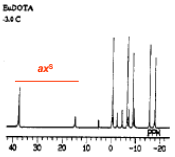

2) Which factors determine SAP/TSAP?

- **Solvent, presence of salts**
- **Number and bulkyness of substituents, eg at pendant arms**
- **Other steric effects**

Solvent effect on SAP/TSAP ratio

LnDOTA-tetraamides

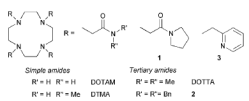

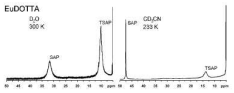

^1H NMR of EuDOTTA in D_2O and CD_3CN ax^S resonances

EuDOTAM: x (SAP) = 0.80 D_2O RT
x (SAP) = 0.97 CD_3CN RT
(Aime et al, *JACS*, 121, 5762-71 (1999))

EuDOTTA: x (SAP) = 0.33 D_2O 273 K
x (SAP) = 0.67 CD_3CN 233 K
(Sherry, 2010)

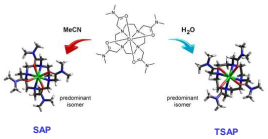

Solvent change increases **SAP** population

Woods and Sherry, *Inorg Chem*, 2010

Steric effects on SAP/TSAP ratio

C(α) substitution with bulky group(s)

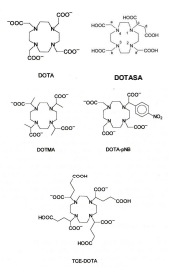

% TSAP (m) isomer increases relative to LnDOTA

Geraldes et al, *Helv Chim Acta*, 88, 633-646 (2005)

^1H NMR of EuDOTASA in D_2O ax^S resonances

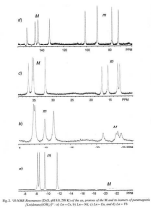

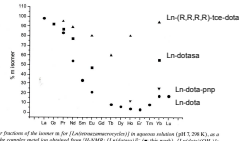

Steric effect on SAP/TSAP ratio

Phosphonate and phosphonate derivative pendant arms cause steric strain: phosphonates have larger byte angle than carboxylates upon Ln^{3+} binding
This causes increase of % TSAP (m or m') and sometimes decrease of q from 1 to 0

Ln-dotp have TSA' structures in solid state and solution

$[Gd(dotp)]^{5-}$
TSA', q = 0

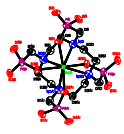

TSA' coordination polyhedron

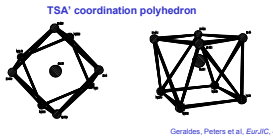

Geraldes, Peters et al, *EurJIC*, 4179-86 (2003)

Ln-do2a2p have TSA/TSA' structures in solid state and solution

$[Ce(H_2do2a2p)(H_2O)]^-$
TSA, q =1

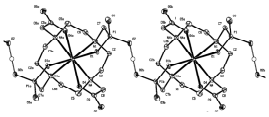

$[Dy(Hdo2a2p)(H_2O)]^{2-}$
TSA', q = 0

Geraldes et al, *Chem Eur J.*, 16, 8446-65 (2010)

DOTP and derivatives - phosphonates and phosphinates

Isomers of Ln(DOTPX)

Chiral elements: R-/S- configurations at each P and helicity (Δ/Λ) of pendant arms
32 stereoisomers = 16 enantiomeric pairs not distinguished by NMR
For 4-fold symmetry (equal pendant arms): 6 diasteroisomers of statistical abundances 1:4:4:2:4:1

Different shapes and energies: populations

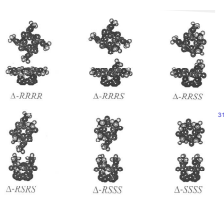

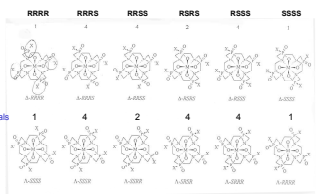

DOTP and derivatives - phosphonates and phosphinates

X-ray structures of Ln(III) complexes

some variation of pendant arm configuration; Gd(III) complexes => q =0

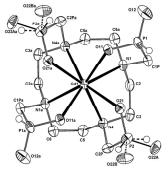

[Gd(DOTP^{H})]$^{-}$: TSA‘

SSSS-Δ–δδδδ (60%, O22A)

SRSR-Δ–δδδδ (40%, O22B)

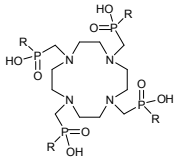

H_4DOTP^R

R = CH_3	H_4DOTP^{Me}
R = CH_2CH_3	H_4DOTP^{Et}
R = C_6H_5	H_4DOTP^{Ph}
R = $CH_2C_6H_5$	H_4DOTP^{Bn}
R = H	H_4DOTP^{H}
R = CH_2OH	H_4DOTP^{hm}
R = OCH_2CH_3	H_4DOTP^{OEt}
R = O-*n*-C_4H_9	H_4DOTP^{OBu}
R = OCH_2CF_3	H_4DOTP^{Otfe}

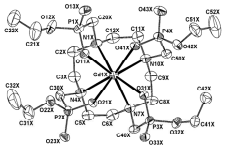

[Gd(DOTPOEt)]$^{-}$

TSA‘

SRSR-Δ–δδδδ

Geraldes et al, *EurJIC*, 119-136 (2009)

NMR of Ln(DOTP^{Et})$^{-}$

Eu(DOTP^{Et})$^{-}$

One major isomer: RRRR >> others, eg. RRRS

Same for Ln(DOTP^{hm})$^{-}$

^{31}P NMR **^{1}H NMR**

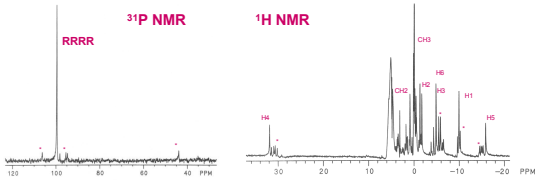

Geraldes et al, *EurJIC*, 119-136 (2009)

^{31}P NMR of Ln(DOTP^{OEt})$^{-}$ and Ln(DOTP^{OBu})$^{-}$

Phosphonate ester complexes

All diasteroisomers present

RRRR ~ SSSS >

RRRS ~ RRSS ~RSSS >

RSRS

Same for Ln(DOTP^{H})$^{-}$

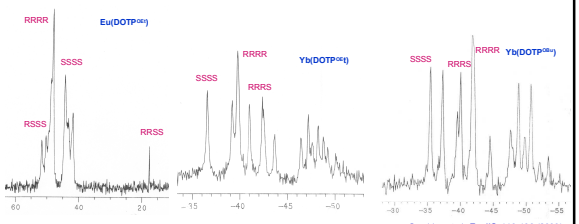

Geraldes et al, *EurJIC*, 119-136 (2009)